



NUMERICAL SIMULATION OF THE UNDER-EXPANDED FLOW IN THE EXPERIMENTAL CONICAL NOZZLE HELIOS-X

SIMULACIÓN NUMÉRICA DEL FLUJO SUBEXPANDIDO EN LA TOBERA CÓNICA EXPERIMENTAL HELIOS-X

San Luis B. Tolentino Masgo^{1,2,*}, Richard Nakka³, Simón Caraballo⁴, Jorge Mírez^{2,5}

Received: 11-03-2020, Reviewed: 22-09-2020, Accepted after review: 17-10-2020

Abstract

Numerical studies of the flow field for convergent-divergent nozzles with throat length, have reported fluctuations of the flow with oblique shock waves in the throat section, for the overexpanded flow condition. However, for other flow conditions, for the same type of nozzle, knowledge is limited. In the present work, the objective is to determine the behavior of the flow in the throat length and in the divergent, for an experimental conical nozzle classified as Helios-X, for the underexpanded flow condition. 2D numerical simulations of the flow field were performed with the ANSYS-Fluent version 12.1 code, applying the RANS model. The governing equations for compressible flow, conservation of mass, momentum, energy, and state were used; as well as, for turbulence, the Menter SST $k - \omega$ model and for the viscosity as a function of temperature the Sutherland equation.

Resumen

Estudios numéricos del campo de flujo para toberas convergentes-divergentes con longitud de garganta, han reportado fluctuaciones del flujo con ondas de choque oblicuo en la sección de la garganta, para la condición de flujo sobre-expandido. Sin embargo, para otras condiciones del flujo, para un mismo tipo de tobera, el conocimiento es limitado. En el presente trabajo, el objetivo es determinar el comportamiento del flujo en la longitud de garganta y en la divergente, para una tobera cónica experimental clasificada como Helios-X, para la condición de flujo sub-expandido. Se realizaron simulaciones numéricas 2D del campo de flujo con el código ANSYS-Fluent versión 12.1, aplicando el modelo RANS. Se emplearon las ecuaciones gobernantes para el flujo compresible, conservación de la masa, cantidad de movimiento, energía y de estado; así como, para la turbulencia el modelo SST $k - \omega$ de Menter y para la viscosidad en función de la temperatura la ecuación de Sutherland.

¹Universidad Nacional Experimental Politécnica Antonio José de Sucre, Vice-Rectorado Puerto Ordaz, Venezuela.

^{2,*}Grupo de Modelamiento Matemático y Simulación Numérica, Universidad Nacional de Ingeniería, Lima, Perú.
Corresponding author: ✉: sanluist@gmail.com. <http://orcid.org/0000-0001-6320-6864>,

³Cohetería experimental amateur, Canadá. <http://orcid.org/0000-0002-7759-7162>

⁴Departamento de Ingeniería Mecánica, Universidad Nacional Experimental Politécnica Antonio José de Sucre Vice-Rectorado Puerto Ordaz, Bolívar, Venezuela. <http://orcid.org/0000-0002-0170-2448>

⁵Facultad de Ingeniería de Petróleo Gas y Petroquímica, Universidad Nacional de Ingeniería, Lima, Perú.
 <http://orcid.org/0000-0002-5614-5853>

In the section of the throat adjacent to the wall the flow exhibited fluctuations; in the axial symmetry the flow showed a stepped acceleration; in the divergent section the flow slowed in a certain region; however, the flow exited the nozzle at a supersonic speed slightly greater than Mach 3. It is concluded that in the throat length section there is a flow pattern, as well as in the divergent section.

Keywords: Throat, Fluctuation, Under-expanded, Simulation, Nozzle.

En la sección de la garganta, adyacente a la pared, el flujo presentó fluctuaciones, en la simetría axial el flujo presentó una aceleración escalonada; en la sección divergente, el flujo se desaceleró en cierta región, sin embargo, el flujo salió de la tobera a velocidad supersónica ligeramente mayor de Mach 3. Se concluye que en la sección de la longitud de garganta se presenta un patrón de flujo, así como, en la sección divergente.

Palabras clave: garganta, fluctuación, subexpandido, simulación, tobera

1. Introduction

The flow in nozzles in supersonic rocket motors is recurrently studied for different geometric configurations of the internal profile of the nozzle walls. The geometry of the divergent section of the nozzle may be conic, bell-shaped, parabolic, rectangular, flat, among others. Taking experimental data in a test bench of the flow within the nozzle in static conditions has limitations when the gas flow is well above the ambient temperature. For this reason, during the experimental test data are recorded with instruments sensitive to changes in pressure, temperature, vibration, in the combustion chamber, at the beginning of the nozzle, in the walls, and through the capture of images of the flow region that is discharged to the environment. When the flow is strangled in the throat and based on the pressure of the combustion chamber, the flow may be overexpanded, optimally expanded or underexpanded [1]. It should be pointed out that, for an overexpanded flow the shock occurs within the nozzle and for an underexpanded flow the shock occurs outside of it.

The experimental data obtained at the boundary of the nozzle are used to reproduce the behavior of the flow field within the nozzle, through the application of computational fluid dynamics [2], [3], which enables quantifying the thermodynamic magnitudes in a computational domain of the flow field that is not possible to obtain by experimental means in open field and labs.

CFD is a computational tool that enables to obtain approximate solutions of the reality of the physical phenomenon, if it is appropriately considered the geometry of the computational domain, the refinement of the mesh, the turbulence model, setting the errors during the iteration stage, as well as other variable control parameters.

For compressible flow there are supported and reported works about the shock waves and the expansion waves of Prandtl-Meyer [4,5], the capturing of images of the shock waves by means of the Schlieren technique [6], the turbulence [7], the limit layer [8,9], as well as the turbulence models [10].

Experimental studies in static and dynamic conditions for convergent-divergent nozzles with throat length have been reported with research purposes; however, the knowledge of the behavior of the flow regime present within nozzles with throat length is virtually none since it has been scarcely addressed using computational tools to determine its thermodynamic magnitudes.

A computational study of the simulation of the overexpanded flow in a conic nozzle with throat length and mean angle of 11° in the divergent section, which belongs to a motor of a sounding rocket for solid fuel, classified as ULA-1A XP [11], reported numerical results of the fluctuations of the flow velocity and of the

oblique shocks that occurred in the throat section, in the range of transonic velocity, as well as the behavior of the flow fluctuation from the center to the walls of the throat. It should be noted that this type of nozzle was previously tested in static and dynamic conditions by the Group of Atmospheric and Space Sciences (GCAE, Grupo de Ciencias de la Atmósfera y del Espacio) of the Universidad de Los Andes, Venezuela [12], [13], [14].

Another study conducted for an underexpanded flow in a conic nozzle with throat length and mean angle of 15° in the divergent section, identified as Helios-X nozzle [15], which also simulated the flow field, presented its results according to the Mach number, where the flow in the throat section exhibited deceleration. Although they provide fundamental data of the flow velocity according to the Mach number, it still remains to analyze with greater detail the flow field for other thermodynamic parameters. For this reason, it is of interest to continue with the investigation for this type of nozzle, to determine the behavior of the field of density, pressure, temperature and velocity, as well as the Mach number in all the domain, and focusing with greater interest in the throat section, which might contribute and enrich the knowledge about the distribution of gradients of the thermodynamic parameters.

The Helios-X nozzle, designed by Nakka [16], was tested in a test bench in static and dynamic conditions. Figure 1 shows the record of the test in static conditions of the nozzle coupled to the Helios-X rocket motor, the rocket in the launching platform and the rocket take-off. Multiple experiments conducted by Nakka of nozzles in rocket motors for amateur solid fuel, in static and dynamic conditions, may be obtained in their web site [16].

The present work is intended to continue with the research for the underexpanded flow in the Helios-X nozzle, reported in [15], with the purpose of determining the behavior of the flow in the throat and divergent sections. In order to achieve the stated objective, the supersonic flow field was simulated to obtain the field of pressure, Mach number, velocity, temperature and density. Results show, in the wall at the inlet of the throat, a region of the flow which exhibits fluctuation, and thus in that region the flow accelerates and decelerates, in other regions of the same section, the flow velocity only slows.

Section 2 presents the equations used, the 2D computational domain and the computational solution method. Section 3 describes the results obtained and the discussion. Section 4 presents the conclusions of the analysis conducted.

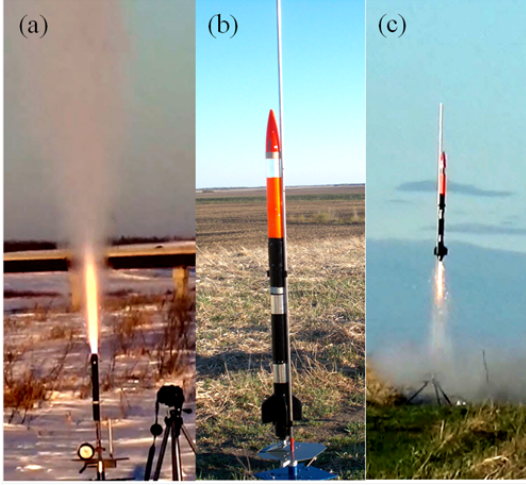


Figure 1. (a) Experimental test in static conditions of the nozzle with throat length coupled to the Helios-X rocket motor, March 2017. (b) Launch platform of the Z-30 rocket, with the Helios-X rocket motor installed. (c) Z-30 rocket take-off, May 2017 [16]

2. Materials and methods

2.1. Mathematical fundamentals

In the present work, the model of the Reynolds-averaged Navier-Stokes (RANS) equations are employed for simulating the flow field of compressible flow. The governing equations used are: the equation of conservation of mass (1), momentum (2), conservation of energy (3), and state (4). In compact form and for a flow in stationary conditions, they are expressed as:

$$\nabla \cdot (\rho u_i) = 0 \quad (1)$$

Where, ρ is the density and u the velocity.

$$\nabla \cdot (\rho u_i u_j) = -\nabla p + \nabla(\bar{\bar{\tau}}) + \nabla \cdot (-\rho \bar{u}_i \bar{u}_j) \quad (2)$$

Where, p is the pressure; $\bar{\bar{\tau}}$ is the tensor of tensions and $-\rho \bar{u}_i \bar{u}_j$ the Reynolds tensions. It should be noted that Equation (2) is closed, since it includes the Reynolds tensions term.

$$\nabla \cdot (u_i (\rho E + p)) = \nabla \cdot (k_{eff} \nabla T + (\bar{\bar{\tau}}_{eff} \cdot u_i)) \quad (3)$$

Where E is the total energy, T the temperature, k_{eff} the effective thermal conductivity, and $\bar{\bar{\tau}}_{eff}$ the effective tensor of tensions.

$$p = \rho R T \quad (4)$$

Where, R is the gas constant.

For compressible flow it is taken into account the ratio of pressures (5) and of temperatures (6) as a function of the Mach number, which is the dominant parameter, and are expressed as:

$$\frac{p_0}{p} = \left(1 + \frac{\gamma - 1}{2} M^2 \right)^{\frac{\gamma}{\gamma - 1}} \quad (5)$$

$$\frac{T_0}{T} = 1 + \frac{\gamma - 1}{2} M^2 \quad (6)$$

Where, p_0 is the total pressure, T_0 the total temperature, γ the ratio of specific heats and M the Mach number.

The supersonic Mach number at the outlet of the nozzle for an underexpanded flow and without shock at the outlet of the divergent section is determined with Equation (7); where A/A^* is the ratio of design areas, A is the area at the outlet of the nozzle and A^* is the area of the throat:

$$\frac{A}{A^*} = \frac{1}{M} \left(\frac{1 + \frac{\gamma - 1}{2} M^2}{\frac{\gamma + 1}{2}} \right)^{\frac{\gamma + 1}{2\gamma - 2}} \quad (7)$$

The considerations of the Mach number are the following: $M < 0.3$ for incompressible flow; $0.3 < M < 0.8$ for subsonic flow; $0.8 < M < 1.2$ for transonic flow; $1.2 < M < 5$ for supersonic flow; $M > 5$ for hypersonic flow; and $M = 1$ for the flow with sonic velocity [5]. It should be noted that White [5] considers that the flow is hypersonic from a value greater than Mach 3, and Anderson [4] from Mach 5.

According to Sutherland's law [8], the viscosity as a function of the temperature (8) is expressed as:

$$\frac{\mu}{\mu_0} = \left(\frac{T}{T_0} \right)^{\frac{3}{2}} \frac{T_0 + S}{T + S} \quad (8)$$

Where, the reference viscosity is $\mu_0 = 1,716 \text{ kg}/(m \cdot s)$, the reference temperature is $T_0 = 273,11 \text{ K}$ and the effective temperature is $S = 110,56 \text{ K}$.

For the flow turbulence, it is taken into account the Menter SST $k - \omega$ turbulence model [17], which is solved together with the equation of momentum. This turbulence model has two equations, one for the specific kinetic energy k , and the other for the specific dissipation rate ω , and thus it improves the responses in the presence of adverse pressure gradients, and flow separation.

The Menter turbulence model [17] has been compared with other turbulence models for different conditions of the compressible flow with presence of shock waves in different experimental equipment for overexpanded flow and underexpanded flow, where the numerical results for 2D domains with symmetric geometries overlap the experimental data of pressure at the walls of experimental equipment, in a nozzle [18,19] and in a transonic diffuser [20,21], with the shapes of the shock

waves of the numerical results approximately similar to the experimental ones. Applications of the Menter turbulence model support their validity for different flow regime conditions [22–25]. In 3D domains, the contribution of the physical analysis is much greater, even for asymmetric geometries and asymmetric lateral loads in the flow field. Therefore, for underexpanded flow conditions and without conditions of asymmetric lateral loads, the Menter turbulence model is appropriate for 2D simulation of the underexpanded flow of the present work.

2.2. Computational domain

The scheme of the geometry of the Helios-X experimental convergent-divergent conic nozzle with throat length [16] is shown in Figure 2, including its main dimensions and corresponding units in millimeters: throat length $L_g = 6.01 \text{ mm}$, throat diameter $D_g = 5.58 \text{ mm}$, ratio between throat length and diameter $r_{LD} = 1.07$, and the ratio of design areas $A/A^* = 5.206$.

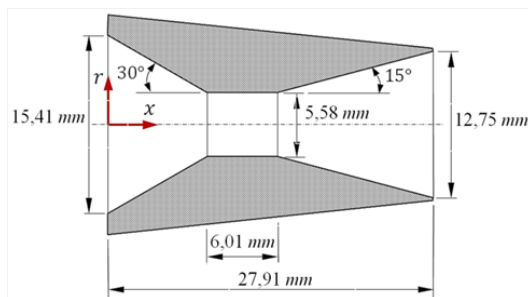


Figure 2. Geometry of the Helios-X experimental conic nozzle [16]

The 2D computational domain with axial symmetry consists of a section of the combustion chamber, the nozzle and the atmosphere, as shown in Figure 3. The purpose of taking into account a short section of 7.47 mm and not the whole section of the motor tube, is to apply the pressure load and direct the flow towards the inlet of the nozzle. The length of the section of the conic nozzle is 27.91 mm and the length of the section of the atmosphere ambient is 281 mm. The throat begins at the position $x=8.51 \text{ mm}$ and ends at the position $x=14.53 \text{ mm}$, and its length is $L_g = 6.01 \text{ mm}$.

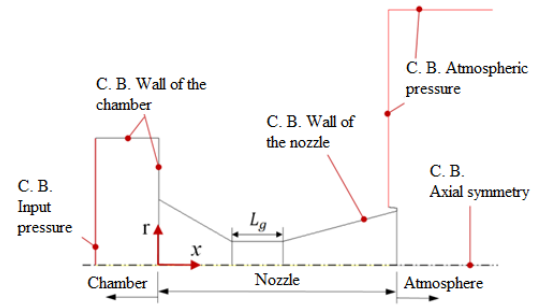


Figure 3. 2D computational domain with axial symmetry. The domain includes a section of the combustion chamber, the nozzle and a section of atmosphere

In addition, since the nozzle has a symmetric revolution geometry, a 2D domain is appropriate, which contributes to reduce the number of cells in the mesh and the iteration time when processing the computational data. In addition, the references where the boundary conditions (BC) are applied are pointed in the same figure of the domain.

The initial and boundary conditions are established as:

In the chamber of the Helios-X rocket motor, the absolute total pressure is established as 6996,11 kPa; and the total temperature as 2558 K.

In the atmosphere ambient, the pressure is established as 101.5 kPa, and the temperature as 263.15 K.

In the axis of axial symmetry, the flow velocity in the radial direction is zero. In the walls, the velocity is zero due to the no-slip condition.

The walls of the section of the combustion chamber and of the nozzle are considered adiabatic.

The effect of the gravity of the flow within the nozzle is not considered, due to the high velocity of the supersonic stream in the divergent. In the atmosphere, the flow velocity is supersonic, and thus for the length of the domain considered, the effect of gravity is considered tiny and therefore neglected.

It should be pointed out that the pressure and temperature data in the chamber of the rocket motor which are applied at the boundary conditions in the present work have been obtained by Nakka [16] through experimental means, as well as the data of the atmosphere ambient recorded with pressure and temperature measuring instruments. The experimental data of the combustion chamber and of the atmosphere ambient applied to the 2D domain, contribute to obtain the simulation of the flow field in all the domain, and enable to determine the behavior of the pressure

and temperature in the wall of the nozzle which has not been possible to measure experimentally.

For the numerical simulations in the present work, the gases burnt as a result of the combustion of the solid propellant consisting of ammonium nitrate, aluminum, sulfur and chloroprene (A24 ANCP) [16] are considered as ideal gases, and as air substance. As parameters, it is fixed the specific heat ratio $\gamma = 1,4$, the gas constant $R = 287 \text{ J}/(\text{kg} \cdot \text{K})$, the specific heat at constant pressure $C_p = 1006,43 \text{ J}/(\text{kg} \cdot \text{K})$ and the thermal conductivity $k = 0,0242 \text{ W}/(\text{m} \cdot \text{K})$.

Figure 4 shows the meshed computational domain and an enlargement of the meshed section of the nozzle. The meshed was made in the ANSYS-Meshing platform and the domain was discretized through the interaction of ICEM-CFD. The mesh of the domain was refined along all the walls, due to the presence of shear stress in those regions. A meshed with triangular cells was applied in the section of the chamber and of the nozzle, and a structured mesh with quadrilateral cells was applied in the section of the atmosphere ambient, for a total of 32675 cells combined. The meshed of the domain shown in the figure is the final one, after performing a numerical convergence study in which the domain was refined three times.

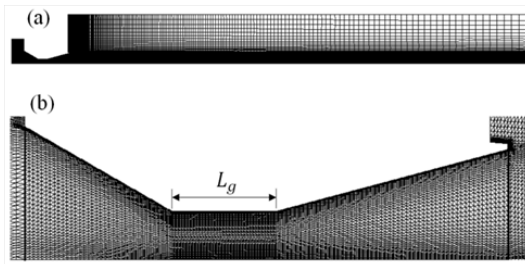


Figure 4. (a) Meshed computational domain with a total of 32675 cells combined. (b) Section of the meshed domain of the nozzle

In the numerical convergence study, the first meshed domain had 30950 cells; in the section of the nozzle the smallest cell had a dimension of $4,9 \times 10^{-5} \text{ mm}$ and the largest one a dimension of $3,37 \times 10^{-4} \text{ mm}$, and the largest cell dimension was 3.2 mm in the upper right corner of the atmosphere domain. The second meshed domain had 32296 cells, with a smallest cell of $4,7 \times 10^{-5} \text{ mm}$ and a largest cell of $3,31 \times 10^{-4} \text{ mm}$, and in the atmosphere domain the maximum cell size was 3.2 mm. The third meshed domain had 32675 cells, with minimum cell dimension of $4,67 \times 10^{-5} \text{ mm}$ and maximum of $3,29 \times 10^{-4} \text{ mm}$, and in the atmosphere the largest cell dimension was 3.2 mm. For the first domain, the minimum spacing of the cell in the wall of the nozzle was $y^+ = 0,98$ in average, for the second domain $y^+ = 0,95$ and for the third domain of the final meshed $y^+ = 0,94$.

For the three cases, the density of the mesh is high in the nozzle and in the region of the atmosphere where

there is the supersonic stream known as plume. The end of the divergent section was taken as control point, in the axial symmetry, to numerically evaluate the Mach number, since it is a critical region due to the high flow velocity, and a percentage error of 0.04% was obtained between the third and second meshed domains; and a slightly larger error of 0.052% between the second and the first, at the outlet of the nozzle in the axial symmetry of the X axis for the third domain of the final meshed and a Mach numeric value of 3.1.

For the theory of quasi-one-dimensional flow with $\gamma = 1,4$, and $A/A^* = 5,206$ of design of the Helios-X nozzle, and without shock at the outlet of the nozzle, a Mach value of 3.217 was obtained with Equation (7) (theoretical). A magnitude difference of 0.117 was obtained between the theoretical Mach number of 3.217 and the Mach of 3.1 numerically calculated of the third meshed domain. Therefore, it is acceptable the magnitude of the result of the comparisons of Mach numbers as numerical validation. For a quasi-one-dimensional and underexpanded flow, the flow exits the nozzle uniformly and perpendicular to the outlet area, and therefore it has the same cross-sectional area, while for the numerical method, the flow has a velocity gradient of the Mach number at the outlet of the nozzle and its magnitude varies in its cross-sectional area.

The meshed domain shown in Figure 4 is appropriate and fulfills satisfactory criteria of the convergence analysis performed. Although the three domains fulfill for $y^+ < 1$, it was chosen the meshed domain with 32675 cells because it has a greater refinement in the walls, which is used in the computational simulations.

The quality of the mesh for two-dimensional cells, and the equiangular bias (Q_{EAS}) establish that it should be in $0 \geq Q_{EAS} \geq 1$, for any 2D cell [26]. For all the domain of the final mesh, it was obtained $Q_{EAS} = 0,55$. It should be stated that the numerical convergence study was performed using the Menter SST $k - \omega$ turbulence model [17] to simulate the flow turbulence.

2.3. Computational solution method

For simulating the flow in the ANSYS-Fluent 12.1 code, which applies the finite volume method (FVM), it was chosen the analysis option based on density for a compressible fluid, 2D domain with axial symmetry in the x axis. For the turbulence of the flow, it was employed the Menter SST $k - \omega$ model [17], and for the viscosity the equation of Sutherland [8].

In the solution method, it was considered the implicit formulation and Roe-FDS type of flow. For the spatial discretization, the gradient: Least Squares Cell based; for the flow, turbulent kinetic energy and the specific dissipation rate, the option: First Order Upwin.

In the residual monitor, for the absolute convergence criterion, it was established a fixed value of

0.00001, for continuity, velocity and energy. It was carried out 136400 iterations in a time close to fifty hours, to obtain the numerical convergence of the final results of the flow field, Mach number, pressure, velocity, temperature and density.

For data processing, an equipment with the following features was employed: Siragon notebook, model M54R, Intel Core 2 Duo, two processors of 1.8 GHz and RAM memory of 3 GB.

3. Results and discussion

This section presents the results of the flow field, for the input pressure load applied of 6996.11 kPa and temperature of 2558 K, ambient pressure at the outlet of the nozzle of 101.5 kPa and temperature of 263.15 K.

The variations of the magnitudes of the static pressure (Figure 5), Mach number (Figure 6), velocity (Figure 7), static temperature (Figure 8) and density (Figure 9), show in which regions of the domain are reached the maximum and minimum values. By means of the contour lines it is observed how they are distributed in different regions of the flow field, both in the section of the nozzle and in the section of the atmosphere.

The flow exiting the nozzle is underexpanded and it is shown in the atmosphere how the shock waves are constituted; and the region of the supersonic stream where these waves are present, is known in the literature as plume.

Figure 10 shows the profiles evaluated in the axial symmetry, for the region of the supersonic flow that exits from the nozzle and discharges in the atmosphere. The fluctuations due to the shock wave are shown, even in certain regions the pressure drops below atmospheric pressure, accelerating the flow in that region before the occurrence of the shock at a Mach value close to 4.75, and velocity of 2050 m/s; while the temperature drops below 500 K. After the shock, the flow is still supersonic with presence of dampen fluctuations around Mach 3, velocity of 1800 m/s and temperature of 900 K. In addition, the behavior of the pressure and density curves show an equilibrium trend.

The contour lines in the nozzle section have been considered, which provide more information regarding the distribution of the gradients of the thermodynamic parameters. The enlarged figures illustrate how the contour lines are distributed in the convergent, throat of length L_g and divergent sections: for the static pressure (Figure 11), Mach number (Figure 12), velocity (Figure 13), static temperature (Figure 14) and density (Figure 15). It is observed that at the beginning of the throat section the contour lines have a behavior different to the contour lines at the end of the same throat, as well as in the middle part.

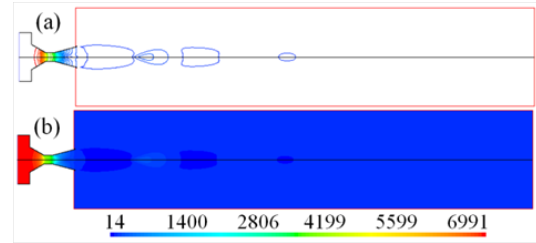


Figure 5. Field of static pressure (kPa)

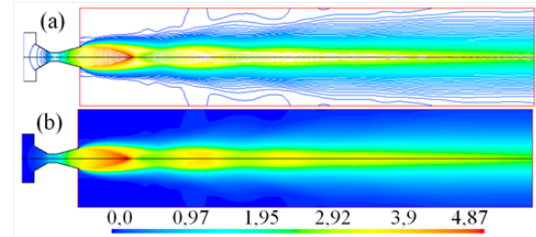


Figure 6. Field of Mach number

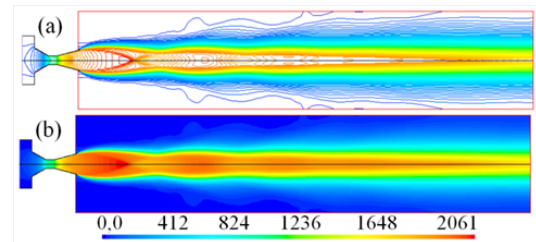


Figure 7. Field of velocity (m/s)

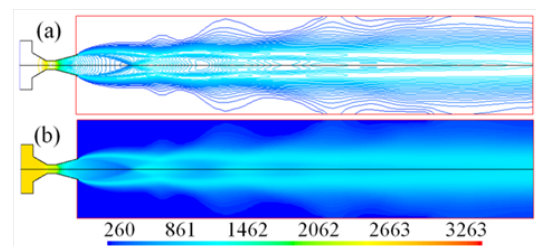


Figure 8. Field of static temperature (K)

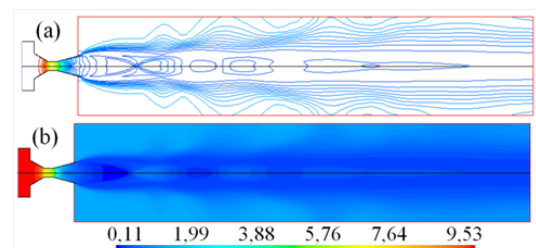


Figure 9. Field of density (kg/m³).

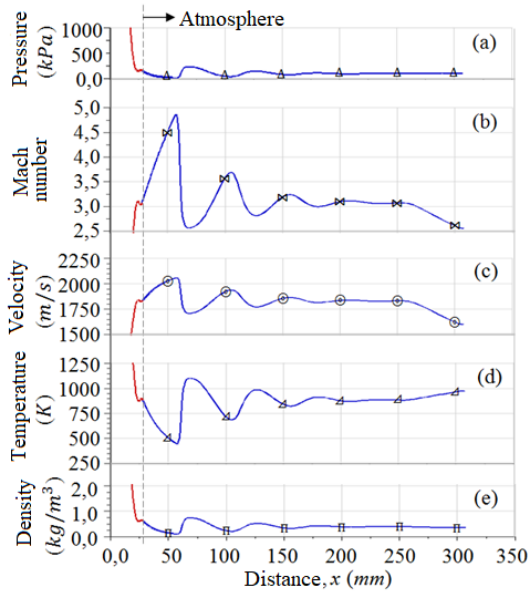


Figure 10. Profiles evaluated in the axial symmetry, in the X axis, in the region of atmosphere ambient. (a) Pressure. (b) Mach number. (c) Velocity. (d) Temperature and (e) Density

It should be pointed out that for the case of static pressure, it is observed that in the middle part of the throat length the contour lines tend to be perpendicular to the walls of the throat, and thus the pressure magnitude in the symmetry is similar to the pressure magnitude in the wall.

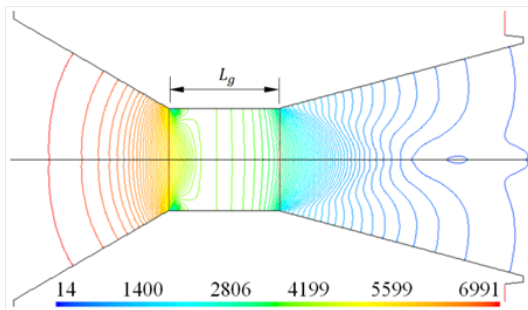


Figure 11. Contour lines of static pressure (kPa) of the flow in the nozzle section

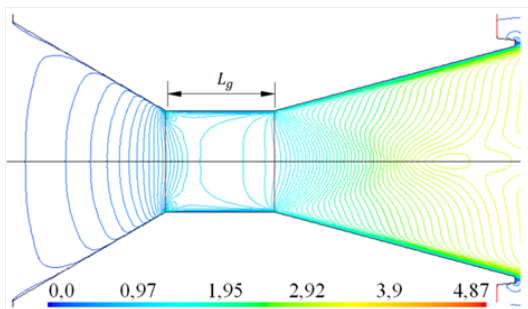


Figure 12. Contour lines of Mach number of the flow in the nozzle section

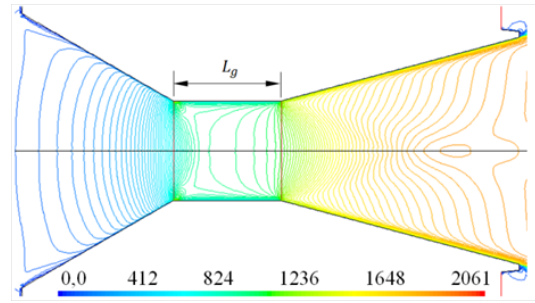


Figure 13. Contour lines of velocity (m/s) of the flow in the nozzle section

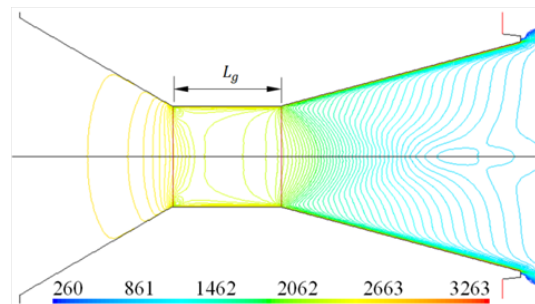


Figure 14. Contour lines of static temperature (K) of the flow in the nozzle section

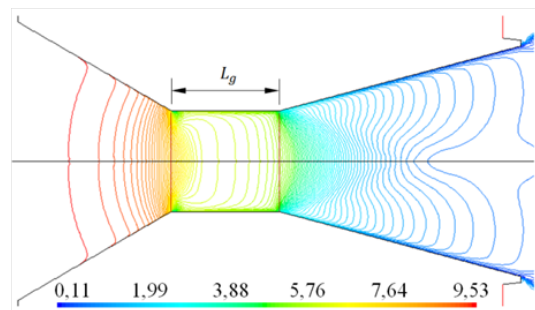


Figure 15. Contour lines of density (kg/m³) of the flow in the nozzle section

Analyzing the behavior of the flow from another perspective, through the trajectory of the numeric curves, it is shown that the sharp change in the static pressure drop (Figure 16) occurs in the first vertex of the throat section. In the middle section of the throat, a part of the trajectories of the pressure profiles in the wall and in the axial symmetry are coincident, which indicates that a uniform flow regime is present with incidence in the acceleration of the flow. Downstream, from position $x=22.5$ mm, the pressure drop of the flow tends to stop, slightly increases, then decreases with smaller intensity, thus being a part of the profile trajectory with oscillatory trend; in such part, the pressure fluctuations influence the development of the

acceleration of the flow, and thus the magnitudes of the thermodynamic parameters exhibit variations.

For the case of the Mach number (Figure 17), it is shown the deceleration of the flow in the throat section, being Mach 1 in the middle part of the throat section, and greater than this value at the outlet of the throat. Close to the outlet of the divergent section, the flow velocity reaches a value greater than Mach 3, at position $x=22.5$ mm, and downstream a curvature is present and tends to reduce the flow up to the outlet of the nozzle, maintaining a velocity greater than Mach 3, corresponding to a supersonic flow. From position $x=22.5$ mm up to the outlet of the nozzle, the behavior of the trajectory of the curve shows that a flow deceleration occurs before exiting the nozzle.

In the velocity profile (Figure 18) it is observed the behavior of the velocity pattern in the axial symmetry, but it is now shown in the wall because the velocity is zero there due to the no-slip condition. In the middle part of the throat section, the flow has an estimated velocity of 920 m/s; downstream, it is shown the behavior of a part of the trajectory of the velocity profile from position $x=22.5$ mm, with a velocity trend slightly greater than 1800 m/s. Also, like in the previous case, for the Mach number the flow velocity decelerates before exiting the nozzle.

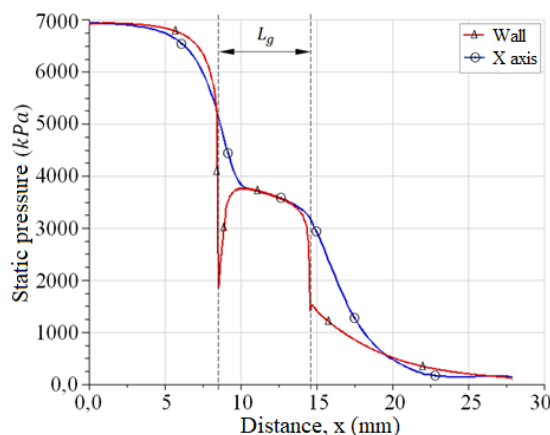


Figure 16. Static pressure profiles evaluated in the wall and in the X axis, in the nozzle section

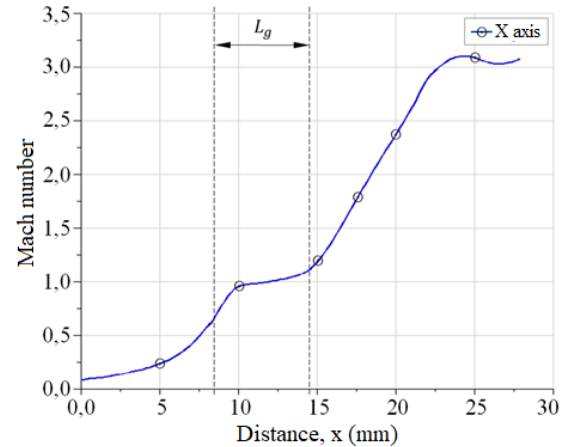


Figure 17. Mach number profile evaluated in the X axis, in the nozzle section

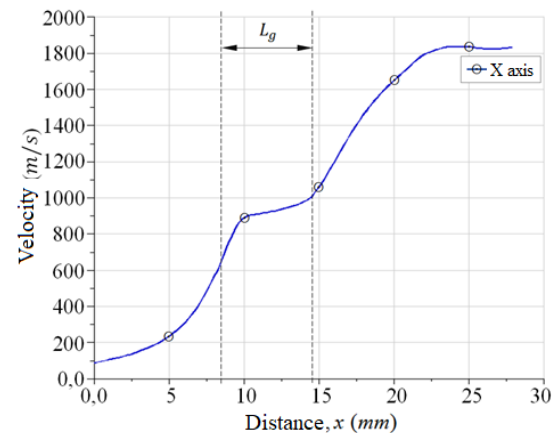


Figure 18. Velocity profile evaluated in the X axis, in the nozzle section

Likewise, for the static temperature profiles (Figure 19), it is shown the behavior of the trajectories in the wall and in the axial symmetry. It is observed in the throat section that the temperature increases and decreases, and the vertices have influence in the occurrence of sudden changes. In the case of the divergent section, the increase of the temperature in the wall to a value greater than the input temperature, is a consequence of the friction of the flow at high velocity rubbing the adiabatic wall, which drastically reduces before the flow exits the nozzle. Whereas in the axial symmetry, the temperature decreases due to the flow expansion, and it is shown the fluctuation of its magnitude from position $x=22.5$ mm. Regarding the density profiles (Figure 20), their behavior depends on the flow expansion and compression, in the convergent, throat and divergent sections.

The results of flow field and of the profiles that define the trajectory of pressure, Mach number, temperature, velocity and density, in the axial symmetry

and in the nozzle wall, are acceptable. This is justified because there is a magnitude difference of 0.117 between the theoretical Mach value of 3.217 obtained with Equation (7) and the numerical value of Mach 3.1 shown in Figure 17, with both values being calculated at the outlet of the nozzle with magnitudes close to each other.

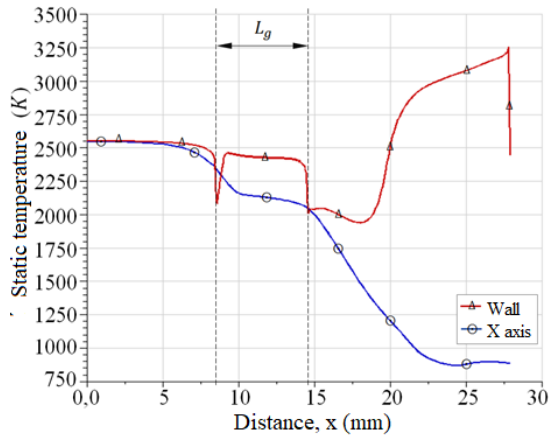


Figure 19. Static temperature profiles evaluated in the wall and in the X axis, in the nozzle section

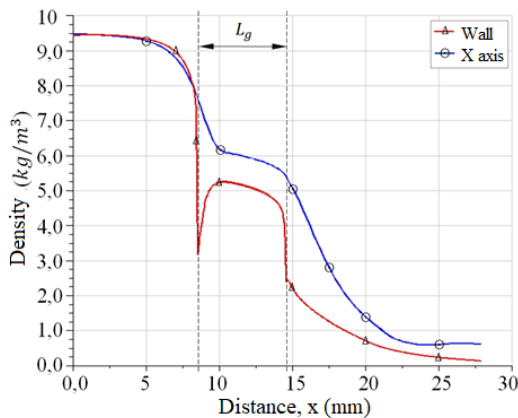


Figure 20. Density profiles evaluated in the wall and in the X axis, in the nozzle section

Enlarged details of the throat section show the behavior of the trajectories of the profiles of static pressure (Figure 21), Mach number (Figure 22), velocity (Figure 23), static temperature (Figure 24) and density (Figure 25), for different radial distances, evaluated from the axial symmetry to the wall. The length of the throat begins at position $x=8.51$ mm and ends at position $x=14.53$ mm. The profiles show the behavior of the flow region in the first vertex, at the beginning of the throat length, along the throat length, as well as when the flow enters at the beginning of the divergent section.

For the case of Mach number (Figure 22) and velocity (Figure 23), for the flow region adjacent to the wall

of the throat section, the flow accelerates, decelerates and accelerates again; whereas in the axial symmetry the flow accelerates, decelerates and accelerates again when entering the divergent section; this is a consequence of the variations in static pressure that occur from the beginning of the throat section up to the end of such section (see Figure 21). Therefore, the geometry of the aerodynamic profile of the throat section of length L_g , determines the behavior of the flow pattern in such section; in this case, there is a flow pattern in the throat section, for an underexpanded flow at the outlet of the nozzle at supersonic velocity greater than Mach 3.

The variations in static temperature in the throat section are shown in Figure 24, where there is an increase of its magnitude in the wall, and variations in the vertices at the inlet and outlet of the throat (Figure 24). Similarly, for the case of the density (Figure 25), its magnitude decreases towards the wall, and in the vertex at the inlet of the throat the density decreases and increases, with a behavior similar to the trajectory of the pressure profile.

Results show that the geometry of the throat section with throat length and diameter ratio $r_{LD}=1.07$, begins at position $x=8.51$ mm and ends at position $x=14.53$ mm, which is a short segment of circular section, has influence on the development of the flow in the regions adjacent to the walls, in the vertices and in the symmetry. In the axial symmetry, in the X axis, the flow reached a value in the range of Mach 0.65 to 1.2, with regions of subsonic, transonic and sonic velocity, without the presence of shocks; therefore, a flow pattern is present.

In a work reported of the ULA-1A XP experimental conic nozzle [11], with mean angle of the divergent section of 11° and throat length and diameter ratio $r_{LD} = 1, 10$, it showed flow deceleration with presence of oblique shock waves, in the range of Mach 0.8 to 1.4; for an overexpanded flow.

When comparing both cases for the flow in the throat region, the length of such region has influence in the development of the flow, either underexpanded or overexpanded flow.

Another flow pattern was present from position $x=22.5$ mm. From position $x=22.5$ mm up to the outlet of the nozzle, the behavior of the trajectory of the curve shows a deceleration of the flow in the divergent section, after the flow reaches the supersonic velocity Mach 3.

Similar results of the flow deceleration in the divergent section for 2D domains, was reported in [19] through a density pattern, for a mean angle of 11.01° of a flat nozzle, for overexpanded flow conditions. Another study reported flow deceleration for a conic nozzle with mean angle smaller than 5° [27], as well as for a nozzle with optimized contour and parabolic contour [28].

Therefore, the fluctuation obtained in the present

work is not an isolated result, since a region of the flow exhibits a deceleration in the divergent section, with a defined pattern.

It should be mentioned that works reported in the literature for inviscid one-dimensional flow [1,4,5,9,26], detail the increase of the flow velocity according to the Mach number in the divergent section of a nozzle, the trajectory of the curve increases and tends to curve towards the outlet of the nozzle, and exhibits no fluctuation. However, the results of the present work show that there is a fluctuation for certain region of the flow in the divergent section, even though the shock wave occurs outside of the nozzle.

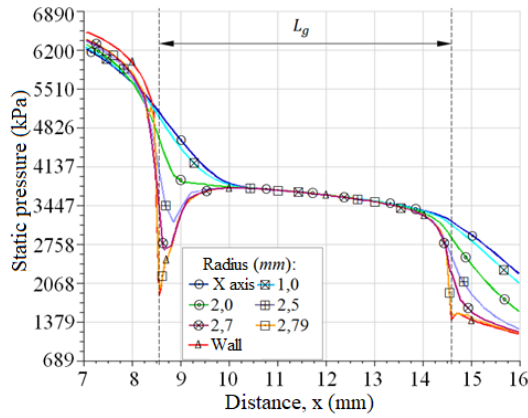


Figure 21. Static pressure profiles evaluated at the throat section of the nozzle

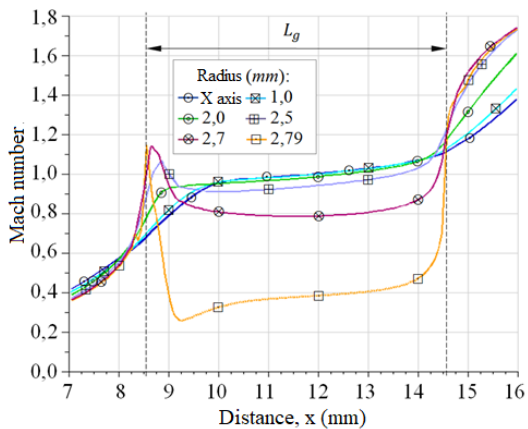


Figure 22. Mach number profiles evaluated at the throat section of the nozzle

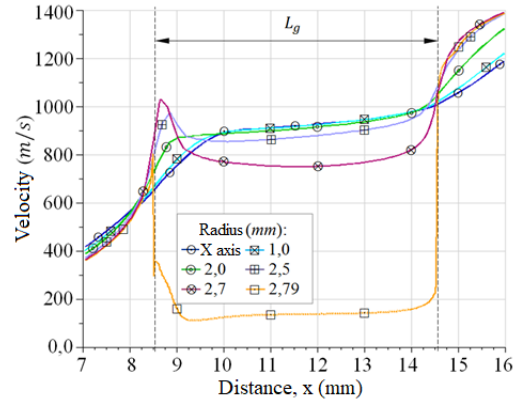


Figure 23. Velocity profiles evaluated at the throat section of the nozzle

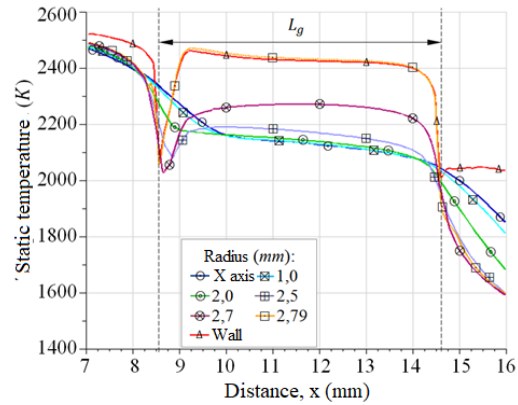


Figure 24. Static temperature profiles evaluated at the throat section of the nozzle

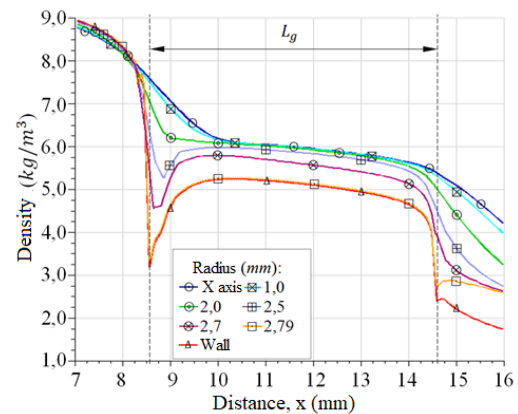


Figure 25. Density profiles evaluated at the throat section of the nozzle

4. Conclusions

According to the analyzes carried out, from the results of the numerical simulations of the underexpanded flow

it is concluded that: In the nozzle section there are two regions where the pressure drop of the flow slows, the throat length section, which is between positions $x=8.51$ mm and $x=14.53$ mm; and at the end of the divergent section, from position $x=22.5$ mm up to the outlet of the nozzle. Therefore, in both regions, the flow decelerates.

In the axial symmetry, at the end of the divergent section of the nozzle, the flow reaches a value slightly larger than Mach 3, and flow velocity of 1800 m/s. In the atmosphere ambient it reaches an estimated value of Mach 4.75, and flow velocity of 2050 m/s, before the occurrence of the shock. Downstream, the magnitudes of Mach number and of velocity fluctuate, up to a prolonged distance around Mach 3.

The profiles of static pressure, Mach number, velocity, static temperature and density, show how the flow develops in the throat section, where at the beginning of such section there is the vertex; a region of the flow adjacent to the wall exhibits fluctuations, causing pressure drops, and thus the flow velocity in such region adjacent to the wall accelerates and decelerates.

In the axial symmetry in the throat, at position $x=8.51$ mm the flow reaches an estimated value of Mach 0.68, and at the end of the throat section, at position $x=14.53$ mm an estimated value of Mach 1.1; thus, a flow region is subsonic, and the rest is transonic. In such section of the throat, the trajectory of the profile defines a staggered behavior.

A future work considers, for 2D and 3D domains and with different computational codes, to progressively reduce the throat length L_g , to determine if there is still influence in the flow acceleration, or if it occurs a possible fluctuation that causes oblique shock waves. Similarly, to determine if the fluctuation of thermodynamic parameters, such as Mach number, pressure and temperature, in the axial symmetry, at the end of the divergent section exhibit some significant change.

Acknowledgements

Mi agradecimiento a Jehová, mi Dios todopoderoso, mi fuente de sabiduría e inspiración. Al Centro de Estudios Energéticos de la Universidad Nacional Experimental Politécnica «AJS» Vice-Rectorado Puerto Ordaz (UNEXPO), Bolívar, Venezuela. Al Grupo de Modelamiento Matemático y Simulación Numérica (GMMNS, Group of Mathematical Modeling and Numerical Simulation) de la Universidad Nacional de Ingeniería (UNI), Lima, Perú. A Richard Nakka (Ingeniero Aeroespacial), por el aporte de datos experimentales de la tobera del motor cohete Helios-X.

References

- [1] G. P. Sutton and O. Biblarz, *Rocket propulsion elements*. John Wiley & Sons, 2016. [Online]. Available: <https://bit.ly/35psFaR>
- [2] J. Blazek, *Computational fluid dynamics: principles and applications*. Butterworth-Heinemann, 2015. [Online]. Available: <https://bit.ly/3pnxjhx>
- [3] B. Andersson, R. Andersson, L. Hakansson, M. Mortensen, R. Sudiyo, and B. van Wachem, *Computational Fluid Dynamics Engineers*. Cambridge University Press, 2011. [Online]. Available: <https://bit.ly/32BPCWo>
- [4] J. D. Anderson, *Fundamentals of aerodynamics*. McGraw-Hill international editions. Mechanical engineering series, 1984. [Online]. Available: <https://bit.ly/3eQR5ge>
- [5] F. M. White, *Fluid Mechanics*. McGraw-Hill series in mechanical engineering, 2011. [Online]. Available: <https://bit.ly/35opmAY>
- [6] P. Krehl and S. Engemann, “August toepfer – the first who visualized shock waves,” *Shock Waves*, vol. 5, no. 1, pp. 1–18, Jun. 1995. [Online]. Available: <https://doi.org/10.1007/BF02425031>
- [7] V. Karman, “The fundamentals of the statistical theory of turbulence,” *Journal of the Aeronautical Sciences*, vol. 4, no. 4, pp. 131–138, 1937. [Online]. Available: <https://doi.org/10.2514/8.350>
- [8] F. White, *Viscous fluid flow*. McGraw-Hill series in Aeronautical and Aerospace Engineering, 1974. [Online]. Available: <https://bit.ly/3eRRCyP>
- [9] H. Schlichting and K. Gersten, *Boundary-Layer Theory*. Springer, 2016. [Online]. Available: <https://bit.ly/36yZGAX>
- [10] D. C. Wilcox, *Turbulence Modeling for CFD*. DCW Industries, Incorporated, 1994. [Online]. Available: <https://bit.ly/32HZnCm>
- [11] A. L. Tolentino, J. Ferreira, M. Parco, L. Lacruz, and V. Marcano, “Simulación numérica del flujo sobre-expandido en la tobera cónica experimental ULA-1A XP,” *Unviversidad, Ciencia y Tecnología*, vol. 21, no. 84, pp. 126–133, 2017. [Online]. Available: <https://bit.ly/2H4yX6k>
- [12] V. Marcano, P. Benitez, C. La Rosa, L. La Cruz, M. A. Parco, J. Ferreira, R. Andrenssen, A. Serra Valls, M. Peñaloza, L. Rodríguez, J. E. Cárdenas, V. Minitti, and J. J. Rojas, “Progresos alcanzados en el proyecto universitario cohete sonda ULA,” *Universidad, Ciencia y Tecnología*, vol. 13, no. 53, pp. 305–316, 2009. [Online]. Available: <https://bit.ly/3f73vB2>

- [13] L. Lacruz-Rincón, M. A. Parco-Brizuela, R. Santos-Luque, C. Torres-Monzón, J. Ferreira-Rodríguez, and P. Benítez-Díaz, “Análisis experimental de las oscilaciones de presión interna en un motor de combustible sólido para cohete sonda,” *Ciencia e Ingeniería*, vol. 13, no. 53, 2016. [Online]. Available: <https://bit.ly/3noQfdL>
- [14] Universidad de los Andes. Programa espacial ULA. [Online]. Available: <https://bit.ly/35tiodw>
- [15] S. L. Tolentino Masgo and R. Nakka, “Simulación del flujo supersónico en la tobera del motor cohete Helios-X de categoría amateur,” in *Jornadas de Investigación*, 2019. [Online]. Available: <https://bit.ly/3pwDY8U>
- [16] R. Nakka. Richard Nakka’s experimental rocketry web site. [Online]. Available: <https://bit.ly/2IrDZKX>
- [17] F. R. Menter, “Two equation eddy-viscosity turbulence models for engineering applications,” *Aerospace Research Central*, vol. 32, no. 8, pp. 1598–1605, 2012. [Online]. Available: <https://doi.org/10.2514/3.12149>
- [18] A. Balabel, A. M. Hegab, M. Nasr, and S. M. El-Behery, “Assessment of turbulence modeling for gas flow in two-dimensional convergent-divergent rocket nozzle,” *Applied Mathematical Modelling*, vol. 35, no. 7, pp. 3408–3422, 2011. [Online]. Available: <https://doi.org/10.1016/j.apm.2011.01.013>
- [19] S. L. Tolentino Masgo, “Evaluación de modelos de turbulencia para el flujo de aire en una tobera plana,” *INGENIUS*, no. 22, pp. 25–37, 2019. [Online]. Available: <https://doi.org/10.17163/ings.n22.2019.03>
- [20] Y. Liu, J. Wu, and L. Lu, “Performance of turbulence models for transonic flows in a diffuser,” *Modern Physics Letters B*, vol. 30, no. 25, p. 1650326, 2016. [Online]. Available: <https://doi.org/10.1142/S0217984916503267>
- [21] S. L. B. Tolentino Masgo, “Evaluación de modelos de turbulencia para el flujo de aire en un difusor transónico,” *Revista Politécnica*, vol. 45, no. 1, pp. 25–38, abr. 2020. [Online]. Available: <https://doi.org/10.33333/rp.vol45n1.03>
- [22] Y. Zhang, H. Chen, M. Zhang, M. Zhang, Z. Li, and S. Fu, “Performance prediction of conical nozzle using navier–stokes computation,” *Journal of Propulsion and Power*, vol. 31, no. 1, pp. 192–203, 2015. [Online]. Available: <https://doi.org/10.2514/1.B35164>
- [23] R. Jia, Z. Jiang, and W. Zhang, “Numerical analysis of flow separation and side loads of a conical nozzle during staging,” *Proceedings of the Institution of Mechanical Engineers, Part G: Journal of Aerospace Engineering*, vol. 230, no. 5, pp. 845–855, 2016. [Online]. Available: <https://doi.org/10.1177/0954410015599798>
- [24] H. Ding, C. Wang, and G. Wang, “Transient conjugate heat transfer in critical flow nozzles,” *International Journal of Heat and Mass Transfer*, vol. 104, pp. 930–942, 2017. [Online]. Available: <https://doi.org/10.1016/j.ijheatmasstransfer.2016.09.021>
- [25] A. K. Mubarak and P. S. Tide, “Design of a double parabolic supersonic nozzle and performance evaluation by experimental and numerical methods,” *Aircraft Engineering and Aerospace Technology*, vol. 91, no. 1, pp. 145–156, Dec. 2020. [Online]. Available: <https://doi.org/10.1108/AEAT-12-2017-0275>
- [26] R. H. Pletcher, J. C. Tannehill, and D. Anderson, *Computational Fluid Mechanics and Heat Transfer*. CRC Press, 2012. [Online]. Available: <https://bit.ly/3psYKX9>
- [27] D. Munday, E. Gutmark, J. Liu, and K. Kailasanath, *Flow Structure of Supersonic Jets from Conical C-D Nozzles*. [Online]. Available: <https://doi.org/10.2514/6.2009-4005>
- [28] J. Östlund and B. Muhammad-Klingmann, “Supersonic Flow Separation with Application to Rocket Engine Nozzles,” *Applied Mechanics Reviews*, vol. 58, no. 3, pp. 143–177, 05 2005. [Online]. Available: <https://doi.org/10.1115/1.1894402>